Magnetic resonance angiography images also clearly showed the structure of the distal MCA branches. The MRA findings of interhemispheric differences with regards to MCA in the SD rat were also consistent with a previous report on Wistar rats [29], which indicated left-to-right asymmetric structure in three out of ten Wistar rats using a 7-T MRI scanner dedicated to small-animal imaging [29]. Our MRA images are superior to those obtained in previous work [11] that employed a clinical 3-T MRI scanner and that only showed the major cerebral arteries and the carotid arteries because they focused mainly on validating occlusion models [11]. The superior quality of our MRA images can largely be attributed to the type of RF coil we used. Ours is a three-turn solenoid coil that covers only the cerebral area, whereas the previous work [11] employed a single-turn coil (diameter of 6.4 cm and length of 10 cm) that covered the whole head, including the brain and the neck. Additionally, the prolonged acquisition period in our study (almost 20 min) compared to the acquisition period used in the previous study [11] (almost 4 min) may have been a factor that led to higher-quality MRA images.

An important point about this study is that DSC-MRI images of reasonable quality can also be obtained with a clinical MRI scanner at 3 T on rats. In addition, we were able to extract the AIF from the rat brain, which is an important accomplishment. Selection of an ROI in the MCA region successfully provided the AIF. Spatial distortion or susceptibility artifacts were not visible in our observations. Signal changes were obtained during DSC-MRI following a single dose of Gd-DTPA. During this study, the dedicated transmit and receive RF coils were considered to be crucial to obtaining a reasonable SNR. Our study was performed with the same sequence and the same dose rate (0.1 mmol/kg) of Gd-DTPA that are commonly used in clinical examinations. Moreover, it was performed with high (1.17 mm^3)-resolution dynamic imaging.

The quantitative images of CBF were consistent with those in a previous report on the use of [^{14}C] iodoantipyrine [30]. Namely, the HT-to-Pt contrast in CBF was 43–52% in this study, which is close to the values reported by Bloom et al. [30] of 44–58%. Although the absolute CBF and CBV values in our study were different from those obtained previously [13, 30, 31], the uncertain scaling factors for each of these were canceled out when calculating the MTT with Eq. 5 [32] (see also the "Appendix"). The MTT obtained in this study was comparable to those obtained in previous work [31, 33].

We noticed that the absolute CBF and CBV values were overestimated, which suggests that some limitations apply, such as the partial volume effect (PVE) caused by insufficient spatial resolution as compared with the anatomic structure of the MCA. Detection of AIF with a repeat injection was performed (Fig. 5, right row). The major MCA diameter was approximately 0.5 mm at the maximum, as evaluated from Fig. 3, which suggested that the measured AIF is largely influenced by the PVE [24]. Also, the differences in absolute value may be due to the fact that a nonlinear relationship exists between the signal intensity and the contrast agent concentration. Previous reports have proposed nonlinearity correction methods for brain tissue [34] and AIF [35]. Further studies are needed to confirm the accuracy and the reproducibility [36]. Image distortion caused by dielectric effects [37] and/or EPI distortion [38] are other sources of error, and should be investigated systematically.

Improving the quality of the original dynamic images acquired would also improve the mapping image quality. In order to achieve better detection of the dynamic susceptibility contrast caused by T_2* signals, the optimization of TE, FA and the acquisition matrix should be investigated. We speculate that a multichannel phased array coil and parallel imaging techniques would reduce the level of distortion. The DSC-MRI in this study was obtained for only a single slice. Further careful attention is needed to perform multislice imaging in order to minimize inflow effects [35]. In our study, the contrast concentration $C(t)$ curves including the AIFs varied slightly among the three injections. A sophisticated injector system that is MR-compatible may improve the variation.

A dedicated high magnetic field scanner equipped with a dedicated small bore is the optimal device for small-animal imaging. However, such systems are not commonly available. The system developed in this study might serve as a low-cost solution or an alternative. The use of the present system provides an opportunity to use the same imaging platform available for clinical studies for small-animal imaging [7]. This would allow us to determine pathophysiological status from MRI signals using animal models with various diseases. More importantly, the optimization of several scan parameters, which has been difficult to achieve in clinical patients, can easily be performed on small animals with this system. In particular, the reproducibility of the assessment of CBF with DSC-MRI, which has been reported to be a limitation on clinical studies [19, 36], could be improved by performing a systematic evaluation of each scan parameter when this system is used on small animals rather than clinical patients. With the addition of a high-strength insert gradient coil [39], which allows for thinner slices and much faster read-out, the system performance and the spatial resolution with an acceptable SNR can be improved. The use of adapting coils could be an effective solution for those who operate MR scanners for human subjects and intend to gain experience [40] in preclinical research.

5 Conclusion

In this preclinical study on rats, reasonable image quality was obtained for T_1W, T_2W, and contrast-free TOF-MRA images generated using a human whole-body 3-T MRI scanner and a newly developed solenoid coil. In DSC-MRI, this system visualized transient signal changes with a single dose of Gd-DTPA and using the same sequences commonly used in clinical examinations. A human whole-body 3-T MRI scanner and dedicated coil make it possible to detect the AIF in the MCA region of Wistar rats. High-resolution DSC-MRI was accomplished with a clinical scanner, but the spatial resolution with an acceptable SNR was insufficient for the rat brain. Although there may be some remaining issues relating to AIF, we have shown the potential of DSC-MRI in our study.

Acknowledgments The authors would like to express our appreciation to the reviewers, the editors and the editorial assistants of *Radiological Physics and Technology* for their invaluable advice on how to improve our manuscript. This study was supported by a grant for research on Advanced Medical Technology from the Ministry of Health, Labor and Welfare, Japan. We would like to thank the VPL released by AZE Ltd. (Tokyo, Japan) and the software library provided by the Oxford University Center for Functional MRI of the Brain. We are grateful to the staff at the National Cardiovascular Center for their invaluable contributions and efforts. Last but not least, we would like to express our thanks to Miss Atra Ardekani (a summer intern from McGill University in Montreal, Quebec, Canada).

Appendix: Calculation of functional mapping images from DSC-MRI

The observed TIC $S(t)$ was converted to a time-versus-concentration curve (TCC) $C(t)$ by the following equation [16, 36]:

$$C(t) = k \cdot \Delta R2^*(t) = -k \cdot \ln(S(0)/S(t))/\mathrm{TE}, \quad (1)$$

where $\Delta R2^*$ is the change in the T_2^* relaxation rate and k is a constant. In this study, it was assumed that $k = 1$. $S(0)$ is the pre-contrast (baseline) signal and $S(t)$ is the measured signal at time t. The next step was to fit this first-pass period of TCC to a gamma variate function:

$$C(t) = a(t-b)^c \exp(-(t-b)/d), \quad (2)$$

where a, b, c, and d were determined by nonlinear least-squares fitting. To minimize the effects of the recirculation of the contrast agent, data were neglected in the fit if these concentrations were less than 50% of the maximum after the peak of the TCC.

The fitted tissue TCC $Ct(t)$ was deconvolved by the fitted AIF $C_{\mathrm{AIF}}(t)$ by using singular value decomposition with a block-circulant deconvolution matrix (b-SVD) method [28] according to the equation

$$\mathrm{CBF} \cdot R(t) = Ct(t) \otimes^{-1} C_{\mathrm{AIF}}(t), \quad (3)$$

where $\otimes^{-1}$ represents the deconvolution operator and $R(t)$ is a residue function representing the tissue response to an instantaneous bolus. $\mathrm{CBF} \cdot R(t)$ was estimated by deconvolving $Ct(t)$ by $C_{\mathrm{AIF}}(t)$ using b-SVD, and then CBF was determined as the maximum value of the obtained $\mathrm{CBF} \cdot R(t)$.

The CBV was calculated as follows:

$$\mathrm{CBV} = \int_0^\infty Ct(t)\mathrm{d}t \Big/ \int_0^\infty C_{\mathrm{AIF}}(t)\mathrm{d}t. \quad (4)$$

Lastly, the MTT is calculated from CBF and CBV by applying the central volume principle [32]:

$$\mathrm{MTT} = \mathrm{CBV}/\mathrm{CBF}. \quad (5)$$

References

1. Brockmann MA, Kemmling A, Groden C. Current issues and perspectives in small rodent magnetic resonance imaging using clinical MRI scanners. Methods. 2007;43:79–87.
2. Smith DA, Clarke LP, Fiedler JA, Murtagh FR, Bonaroti EA, Sengstock GJ, et al. Use of a clinical MR scanner for imaging the rat brain. Brain Res Bull. 1993;31(1–2):115–20.
3. Guzman R, Lövblad KO, Meyer M, Spenger C, Schroth G, Widmer HR. Imaging the rat brain on a 1.5 T clinical MR-scanner. J Neurosci Methods. 2000;97(1):77–85.
4. Fujioka M, Taoka T, Matsuo Y, Hiramatsu KI, Sakaki T. Novel brain ischemic change on MRI: delayed ischemic hyperintensity on T_1-weighted images and selective neuronal death in the caudoputamen of rats after brief focal ischemia. Stroke. 1999;30(5):1043–6.
5. Thorsen F, Ersland L, Nordli H, Enger PO, Huszthy PC, Lundervold A, et al. Imaging of experimental rat gliomas using a clinical MR scanner. J Neurooncol. 2003;63(3):225–31.
6. Biswas J, Nelson CB, Runge VM, Wintersperger BJ, Baumann SS, Jackson CB, et al. Brain tumor enhancement in magnetic resonance iimaging: comparison of signal-to-noise ratio (SNR) and contrast-to-noise ratio (CNR) at 1.5 versus 3 Tesla. Invest Radiol. 2005;40:792–7.
7. Shimamura M, Sato N, Sata M, Kurinami H, Takeuchi D, Wakayama K, et al. Delayed postischemic treatment with fluvastatin improved cognitive impairment after stroke in rats. Stroke. 2007;38:3251–8.
8. Lee JM, Zhai G, Liu Q, Gonzales ER, Yin K, Yan P, et al. Vascular permeability precedes spontaneous intracerebral hemorrhage in stroke-prone spontaneously hypertensive rats. Stroke. 2007;38:3289–91.
9. Wintersperger BJ, Runge VM, Biswas J, Reiser MF, Schoenberg SO. Brain tumor enhancement in mr imaging at 3 Tesla: comparison of SNR and CNR gain using TSE and GRE techniques. Invest Radiol. 2007;42:558–63.
10. Sato H, Enmi J, Teramoto N, Hayashi T, Yamamoto A, Tsuji T, et al. Comparison of Gd-DTPA-induced signal enhancements in rat brain C6 glioma among different pulse sequences in 3-Tesla magnetic resonance imaging. Acta Radiol. 2008;49:172–9.
11. Yang YM, Feng X, Yao ZW, Tang WJ, Liu HQ, Zhang L. Magnetic resonance angiography of carotid and cerebral arterial

occlusion in rats using a clinical scanner. J Neurosci Methods. 2008;167(2):176–83.
12. Rosen BR, Belliveau JW, Vevea JM, Brady TJ. Perfusion imaging with NMR contrast agents. Magn Reson Med. 1990;14(2):249–65.
13. Calamante F, Thomas DL, Pell GS, Wiersma J, Turner R. Measuring cerebral blood flow using magnetic resonance imaging techniques. J Cereb Blood Flow Metab. 1999;19(7):701–35.
14. Yamada K, Wu O, Gonzalez RG, Bakker D, Østergaard L, Copen WA, et al. Magnetic resonance perfusion-weighted imaging of acute cerebral infarction: effect of the calculation methods and underlying vasculopathy. Stroke. 2002;33(1):87–94.
15. Tamura H, Hatazawa J, Toyoshima H, Shimosegawa E, Okudera T. Detection of deoxygenation-related signal change in acute Ischemic stroke patients by T2*-weighted magnetic resonance imaging. Stroke. 2002;33(4):967–71.
16. Calamante F, Gadian DG, Connelly A. Quantification of perfusion using bolus tracking magnetic resonance imaging in stroke: assumptions, limitations, and potential implications for clinical use. Stroke. 2002;33(4):1146–51.
17. Latchaw RE, Yonas H, Hunter GJ, Yuh WT, Ueda T, Sorensen AG, et al. Guidelines and recommendations for perfusion imaging in cerebral ischemia: a scientific statement for healthcare professionals by the Writing Group on Perfusion Imaging, from the Council on Cardiovascular Radiology of the American Heart Association. Stroke. 2003;34(4):1084–104.
18. Carroll TJ, Rowley HA, Haughton VM. Automatic calculation of the arterial input function for cerebral perfusion imaging with MR imaging. Radiology. 2003;227(2):593–600.
19. Wintermark M, Sesay M, Barbier E, Borbély K, Dillon WP, Eastwood JD, et al. Comparative overview of brain perfusion imaging techniques. Stroke. 2005;36(9):83–99.
20. Bruening R, Kwong KK, Vevea MJ, Hochberg FH, Cher L, Harsh GR 4th, et al. Echo-planar MR determination of relative cerebral blood volume in human brain tumors: T1 versus T2 weighting. AJNR Am J Neuroradiol. 1996;17(5):831–40.
21. Chen F, Suzuki Y, Nagai N, Peeters R, Coenegrachts K, Coudyzer W, et al. Visualization of stroke with clinical MR imagers in rats: a feasibility study. Radiology. 2004;233:905–11.
22. Chen F, Suzuki Y, Nagai N, Sun X, Coudyzer W, Yu J, et al. Delayed perfusion phenomenon in a rat stroke model at 1.5 T MR: An imaging sign parallel to spontaneous reperfusion and ischemic penumbra? Eur J Radiol. 2007;61:70–8.
23. Fan G, Zang P, Jing F, Wu Z, Guo Q. Usefulness of diffusion/perfusion-weighted MRI in rat gliomas: correlation with histopathology. Acad Radiol. 2005;12(5):640–51.
24. van Osch MJ, van der Grond J, Bakker CJ. Partial volume effects on arterial input functions: shape and amplitude distortions and their correction. J Magn Reson Imaging. 2005;22(6):704–9.
25. Wada Y, Hara T, Miyati T. Basic assessment of the CNR measurement method of MRI system in phantom—suggestion for improvement in the CNR evaluation method. Nippon Hoshasen Gijutsu Gakkai Zasshi. 2008;64(2):268–76.
26. Ogura A, Maeda F, Miyai A, Hongoh T. Accuracy of contrast-to-noise ratio measurement for magnetic resonance clinical images. Nippon Hoshasen Gijutsu Gakkai Zasshi. 2004;60(11):1543–9.
27. Miyati T. Image quality assessment in magnetic resonance imaging. Nippon Hoshasen Gijutsu Gakkai Zasshi. 2002;58(1):40–8.
28. Wu O, Ostergaard L, Weisskoff RM, Benner T, Rosen BR, Sorensen AG. Tracer arrival timing-insensitive technique for estimating flow in MR perfusion-weighted imaging using singular value decomposition with a block-circulant deconvolution matrix. Magn Reson Med. 2003;50:164–74.
29. Besselmann M, Liu M, Diedenhofen M, Franke C, Hoehn M. MR angiographic investigation of transient focal cerebral ischemia in rat. NMR Biomed. 2001;14(5):289–96.
30. Bloom AS, Tershner S, Fuller SA, Stein EA. Cannabinoid-induced alterations in regional cerebral blood flow in the rat. Pharmacol Biochem Behav. 1997;57(4):625–31.
31. Shockley RP, LaManna JC. Determination of rat cerebral cortical blood volume changes by capillary mean transit time analysis during hypoxia, hypercapnia and hyperventilation. Brain Res. 1998;454(1–2):170–8.
32. Meier P, Zierler KL. On the theory of the indicator-dilution method for measurement of blood flow and volume. J Appl Physiol. 1954;6:731–44.
33. Johansson E, Månsson S, Wirestam R, Svensson J, Petersson JS, Golman K, et al. Cerebral perfusion assessment by bolus tracking using hyperpolarized 13C. Magn Reson Med. 2004;51(3):464–72.
34. Enmi J, Hayashi T, Watabe H, Moriwaki H, Yamada N, Iida H. Measurement of cerebral blood flow with dynamic susceptibility contrast MRI and comparison with O-15 positron emission tomography. Int Congr Ser. 2004;1265:150–8.
35. Calamante F, Vonken EJ, van Osch MJ. Contrast agent concentration measurements affecting quantification of bolus-tracking perfusion MRI. Magn Reson Med. 2007;58:544–53.
36. Grandin CB, Bol A, Smith AM, Michel C, Cosnard G. Absolute CBF and CBV measurements by MRI bolus tracking before and after acetazolamide challenge: repeatability and comparison with PET in humans. Neuroimage. 2005;26:525–35.
37. Kuhl CK, Träber F, Schild HH. Whole-body high-field-strength (3.0-T) MR imaging in clinical practice. Part I. Technical considerations and clinical applications. Radiology. 2008;246(3):675–96.
38. Jezzard P, Clare S. Sources of distortion in functional MRI data. Hum Brain Mapp. 1999;8(2–3):80–5.
39. Mayer D, Zahr NM, Adalsteinsson E, Rutt B, Sullivan EV, Pfefferbaum A. In vivo fiber tracking in the rat brain on a clinical 3T MRI system using a high strength insert gradient coil. Neuroimage. 2007;35(3):1077–85.
40. Graf H, Martirosian P, Schick F, Grieser M, Bellemann ME. Inductively coupled rf coils for examinations of small animals and objects in standard whole-body MR scanners. Med Phys. 2003;30(6):1241–5.

Journal of Cerebral Blood Flow & Metabolism (2008), 1–10

www.jcbfm.com

A physiologic model for recirculation water correction in $CMRO_2$ assessment with $^{15}O_2$ inhalation PET

Nobuyuki Kudomi, Takuya Hayashi, Hiroshi Watabe, Noboru Teramoto, Rishu Piao, Takayuki Ose, Kazuhiro Koshino, Youichirou Ohta and Hidehiro Iida

Department of Investigative Radiology, Advanced Medical-Engineering Center, National Cardiovascular Center Research Institute, Osaka, Japan

Cerebral metabolic rate of oxygen ($CMRO_2$) can be assessed quantitatively using $^{15}O_2$ and positron emission tomography. Determining the arterial input function is considered critical with regards to the separation of the metabolic product of $^{15}O_2$ (RW) from a measured whole blood. A mathematical formula based on physiologic model has been proposed to predict RW. This study was intended to verify the adequacy of that model and a simplified procedure applying that model for wide range of species and physiologic conditions. The formula consists of four parameters, including of a production rate of RW (*k*) corresponding to the total body oxidative metabolism ($BMRO_2$). Experiments were performed on 6 monkeys, 3 pigs, 12 rats, and 231 clinical patients, among which the monkeys were studied at varied physiologic conditions. The formula reproduced the observed RW. Greater *k* values were observed in smaller animals, whereas other parameters did not differ amongst species. The simulation showed $CMRO_2$ sensitive only to *k*, but not to others, suggesting that validity of determination of only *k* from a single blood sample. Also, *k* was correlated with $BMRO_2$, suggesting that *k* can be determined from $BMRO_2$. The present model and simplified procedure can be used to assess $CMRO_2$ for a wide range of conditions and species.
Journal of Cerebral Blood Flow & Metabolism advance online publication, 5 November 2008; doi:10.1038/jcbfm.2008.132

Keywords: arterial input; $CMRO_2$; mathematical modeling; recirculation water; PET

Introduction

Cerebral metabolic rate of oxygen ($CMRO_2$) can be quantitatively assessed using ^{15}O-labeled oxygen ($^{15}O_2$) and positron emission tomography (PET). This technique is based on an estimation of influx rate of $^{15}O_2$ to the cerebral tissue from arterial blood. Using information of cerebral blood flow (CBF) that may be obtained either from a separate scan with ^{15}O-labeled water ($H_2^{15}O$) or from the clearance rate $^{15}O_2$ of tissue, the oxygen extraction fraction (OEF) can also be calculated. The arterial input function must be determined before beginning this calculation. More specifically, a metabolic product of $^{15}O_2$ in the arterial blood, as a form of ^{15}O-labeled water (i.e., recirculating ^{15}O-water or RW) needs to be accurately estimated.

The arterial whole blood radioactivity curve can be obtained by measuring the radioactivity concentration of continuously withdrawn whole blood using a monitoring device (Eriksson *et al*, 1988; Eriksson and Kanno, 1991; Votaw and Shulman, 1998; Kudomi *et al*, 2003). Assessment of a time-dependent RW curve may be achieved by separating the plasma from the whole blood samples. This, however, requires labor-intensive procedures of frequent, manual arterial blood samplings, the centrifugation of all collected blood samples, and radioactivity measurements for both whole blood and plasma (Holden *et al*, 1988).

Ohta *et al* (1992) proposed to neglect the component of RW from the arterial input function. This technique fits three parameters of $CMRO_2$, CBF, and

Correspondence: Dr H Iida, Department of Investigative Radiology, Advanced Medical-Engineering Center, National Cardiovascular Center Research Institute, 5-7-1, Fujishirodai, Suita, Osaka 565-8565, Japan.
E-mail: iida@ri.ncvc.go.jp
This study was supported by the Program for Promotion of Fundamental Studies in Health Science of the Organization for Pharmaceutical Safety and Research of Japan, a Grant for Research on Advanced Medical Technology from the Ministry of Health, Labour and Welfare (MHLW), Japan, and by Nakatani Electronic Measuring Technology Association of Japan (NK).
Received 2 May 2005; revised 6 October 2008; accepted 11 October 2008

cerebral blood volume (CBV) to the kinetic $^{15}O_2$ data obtained from a single PET scan after the bolus administration of $^{15}O_2$. To minimize errors which result from neglecting RW, only the initial 3 mins of data after the bolus inhalation of $^{15}O_2$ were used when calculating the parameters. This approach has been applied to evaluate the magnitude of increase in $CMRO_2$ relative to that in CBF during cognitive stimulation tasks (Fujita *et al*, 1999; Vafaee and Gjedde, 2000; Okazawa *et al*, 2001*a*, *b*; Yamauchi *et al*, 2003; Mintun *et al*, 2002), but one of the drawbacks to this technique is the lack of accurate statistics, which is due to the use of a short scan duration.

Iida *et al* (1993) have developed a mathematical formula to predict the production of RW based on a physiologic model, which allows prolongation of the PET acquisition period with an additional statistical accuracy. The formula assumes a fixed rate constant for production of RW from $^{15}O_2$ in the body. This is based on the fact that the observed rate constant did not vary among clinical subjects, and thus causes nonsignificant errors in $CMRO_2$. However, the study is limited only to human subjects studied at rest, and results have not been verified using other species such as rat and mouse (Magata *et al*, 2003; Temma *et al*, 2006; Yee *et al*, 2006). Also, the findings have not been evaluated on humans who are under physiologic stress, though under such conditions the whole-body oxygen consumption is expected to change. Moreover, it is important to extend the approach to physiologically stressed conditions as recent progress for assessing $CMRO_2$ and CBF simultaneously from a short period dynamic scan by using a dual tracer autoradiography (DARG) (Kudomi *et al*, 2005). The DARG has enabled the $^{15}O_2$ PET to assess $CMRO_2$ and CBF simultaneously at various physiologically activated conditions.

The aim of this study is to verify the method used to estimate the arterial RW during the $^{15}O_2$ inhalation for simultaneous determination of $CMRO_2$ and CBF from the rapid procedures of $^{15}O_2$ PET. The feasibility of a simplified procedure is also being investigated. Applicability of this approach was tested for a wide range of species under various physiologic conditions. Experiments were designed to apply for different species as well as different physiologic conditions. A simulation study was also performed to evaluate the level of error sensitivity associated with this approach.

Materials and methods

Theory

Variables used in the recirculating water model are summarized in Table 1. The mathematical model that formulates the time-dependent RW in arterial blood consists of three rate constants: (1) the production rate of RW or k (per min), proportional to oxidative metabolism in the total body system ($BMRO_2$), (2) the forward diffusion rate (k_w, per min) of the metabolized ^{15}O-water between the blood and interstitial spaces in the body, and (3) the backward diffusion rate (k_2, per min) of the metabolized ^{15}O-water between the blood and interstitial spaces in the body. The differential equations for the arterial activity concentration of ^{15}O-water at a time t (secs) ($A_w(t)$, Bq/mL), after the physical decay correction can be expressed as follows (Huang *et al*, 1991):

$$\frac{d}{dt}A_w(t) = k \cdot A_o(t) - k_w \cdot A_w(t) + k_2 \cdot C(t) \quad (1a)$$

$$\frac{d}{dt}C(t) = k_w \cdot A_w(t) - k_2 \cdot C(t) \quad (1b)$$

$$A_t(t) = A_o(t) + A_w(t) \quad (1c)$$

where $A_o(t)$ and $A_t(t)$ denote the radioactivity concentration of the arterial $^{15}O_2$ and the total radioactivity from both

Table 1 Variables used in the recirculating water model

Symbol	*Description*	*Unit*
A_o	Radioactivity concentration of arterial $^{15}O_2$	Bq/mL
A_w	Radioactivity concentration of arterial $H_2^{15}O$	Bq/mL
A_t	Total radioactivity concentration from arterial $^{15}O_2$ and $H_2^{15}O$	Bq/mL
A_{plasma}	Radioactivity concentration of arterial plasma	Bq/mL
C	Activity concentration of $H_2^{15}O$ in peripheral tissue in a body	Bq/mL
Fi_{O_2}	Oxygen concentration in inhaled gas	%
Fe_{O_2}	Oxygen concentration in expired gas	%
k	Production rate of recirculating $H_2^{15}O$	per min
k_{BM}	Production rate of recirculating $H_2^{15}O$ obtained from BM approach	per min
k_w	Forward diffusion rate of $H_2^{15}O$ from blood to body interstitial space	per min
k_2	Backward diffusion rate of $H_2^{15}O$ from blood to body interstitial space	per min
λ	Decay constant of ^{15}O (=0.00567 per sec)	per sec
v	Stroke volume	mL
p	k_w/k_2	
r	Respiration rate	per min
R	Fractional water content ratio in whole blood to that in the plasma	
R_{O_2}	Rate of oxidative metabolism in the whole-body system	mL/min
Δt	Delayed appearance time of recirculating water	secs
V_{O_2}	Total volume of molecular oxygen in total blood	mL
V_{TB}	Total volume of blood in a body	mL

$^{15}O_2$ and $H_2^{15}O$, respectively. $C(t)$ is an activity concentration of $H_2^{15}O$ in the peripheral tissue of the total body. Assuming a delayed appearance of RW by Δt (Iida *et al*, 1993), the following equation can be obtained:

$$A_w(t+\Delta t) = k(\alpha_1 \cdot A_t(t) \otimes \exp(-\beta_1 t) + \alpha_2 \cdot A_t(t) \otimes \exp(-\beta_2 t)) \quad (2)$$

where $\otimes$ denotes the convolution integral and:

$$\alpha_{1.2} = \frac{a - 2c \pm \sqrt{a^2 - 4b}}{\pm 2\sqrt{a^2 - 4b}}, \qquad \beta_{1.2} = \frac{a \pm \sqrt{a^2 - 4b}}{2},$$
$$a = k + k_w + k_w/p, \quad b = k \cdot k_w/p, \quad c = k_w/p; \quad p = k_w/k_2 \quad (3)$$

Following four approaches were performed to determine the rate constants and $A_w(t)$.

Approach by four parameters fitting: Four parameters, k, Δt, k_w, and p ($=k_w/k_2$), can be determined from the observed RW ($A_w(t)$) and the $A_t(t)$ curves by means of the nonlinear least square fitting (4PF approach).

Approach by one parameter fitting: Once three parameters, Δt, k_w, and p, are fixed by averaging values determined by the 4PF approach, k can then be determined by fitting the Equation 2 to measured $A_w(t)$ from $A_t(t)$ (1PF approach). In this procedure, single datum is sufficient, and thus k can be determined from $A_t(t)$ and the RW counts sampled at a single time point.

Approach from steady-state condition: Similarly to the 1PF procedures, k can be determined from the steady state condition, which is achieved by a continuous administration of $^{15}O_2$ as follows (SS approach). Incorporating the decay constant of ^{15}O ($\lambda = 0.00567$ per secs) into Equations 1a and 1b provides:

$$\frac{d}{dt}A^*_w(t) = k \cdot A^*_o(t) - k_w \cdot A^*_w(t) + k_2 \cdot C^*(t) - \lambda \cdot A^*_w(t) \quad (4a)$$

$$\frac{d}{dt}C^*(t) = k_w \cdot A^*_w(t) - k_2 \cdot C^*(t) - \lambda \cdot C^*(t) \quad (4b)$$

where variables with the symbol * denote that no correction was made for the radioactivity decay of ^{15}O. After continuously administrating $^{15}O_2$, the radioactivity distribution of $A^*_o(t)$, $A^*_w(t)$, and $C^*_t(t)$ reaches a steady state. Thus, the following equations hold:

$$0 = k \cdot A^*_o(t) - k_w A^*_w(t) + k_2 C^*(t) - \lambda A^*_w(t) \quad (5a)$$

$$0 = k_w A^*_w(t) - k_2 C^*(t) - \lambda C^*(t) \quad (5b)$$

Given the values of k_w and k_2 which are determined as averages of 4PF, k can be calculated from the arterial $^{15}O_2$ and $H_2^{15}O$ concentrations at steady state as follows:

$$k = \lambda\left(\frac{k_w + k_2 + \lambda}{k_2 + \lambda}\right)\frac{A^*_w(t)}{A^*_o(t)} \quad (6)$$

Approach by the rate of whole body oxidative metabolism: In this study, an alternative approach is provided to obtain k, from the rate of oxidative metabolism in the whole-body system (BM approach). With this alternative approach, we assume that the production rate of RW or k is proportional to the rate of oxidative metabolism in the whole-body system (i.e., $BMRO_2$ (R_{O_2}, mL/min)). The rate of oxidative metabolism may change dependent on physiologic status of the subject. In addition, we assumed that this index can be defined from the difference of oxygen concentration between inhaled and exhaled trachea air samples. Therefore, the above can be expressed as follows:

$$k = c \cdot \frac{R_{O_2}}{V_{O_2}} \ (\text{per min}) \quad (7a)$$

or

$$k_{BM} = \frac{k}{c} = \frac{R_{O_2}}{1.36 \cdot Hb \cdot V_{TB}} \quad (7b)$$

where c is the proportionality constant, k_{BM} the production rate of RW obtained from BM approach, V_{O_2} (mL) the total volume of molecular oxygen in total blood, 1.36 mL/g the amount of oxygen molecules combined with unit mass of hemoglobin, Hb (g/mL) represents the hemoglobin concentration in the arterial blood, and V_{TB} (mL) is the total volume of blood in the body.

Simulation

A series of simulation studies were performed to investigate the effects of errors on estimated $CMRO_2$ value in the model parameters (k, Δt, k_w, and p). In these simulations, a typical arterial blood time activity curve (TAC) of $^{15}O_2$ and $H_2^{15}O$ after DARG protocol (Kudomi *et al*, 2005) obtained in a monkey study was used. RW TACs were generated from the whole blood TAC by assuming baseline values of k as 0.13, 0.11, 0.34, and 0.73 per min, Δt as 20, 11, 5, and 3 secs, k_w as 0.38, 0.43, 0.98, and 0.87 per min, and p as 1.31, 1.01, 0.98, and 0.83, corresponding to humans, pigs, monkeys, and rats, respectively. Tissue TACs were generated by assuming CBF = 50 mL/min per 100 g and OEF = 0.4 ($CMRO_2$ was defined as: $CMRO_2 = CBF \times OEF \times C_aO_2$, where C_aO_2 is the arterial oxygen content. This simulation was intended to investigate magnitude of error as a percentage difference, so that arbitrary value of C_aO_2 was assumed) (Hayashi *et al*, 2003), using a kinetic formula for oxygen and water in the brain tissue (Mintun *et al*, 1984; Shidahara *et al*, 2002; Kudomi *et al*, 2005). $CMRO_2$ values were calculated by the DARG method (Kudomi *et al*, 2005), in which RW TACs were separated from the whole blood by changing k from 0.0 to 1.0 per min, Δt from 0 to 30 secs, k_w from 0.0 to 2.0 per min, and p from 0.0 to 2.0, respectively. Errors in the estimated $CMRO_2$ were presented as a percentage difference from the assumed true values.

Subjects

Subjects consisted of four groups including monkeys, pigs, rats, and clinical patients. Monkeys were six healthy *macaca fascicularis* with body weight of 5.2 ± 0.8 kg and age ranging from 3- to 4-year old. Pigs were three farm pigs

with body weight of 38 ± 9 kg and age from 4 to 12 months. Rats were 12 male Wistar rats with body weight of 300 ± 54 g and age from 7 to 8 weeks. All animals were studied during anesthesia. The animals were maintained and handled in accordance with guidelines for animal research on Human Care and Use of Laboratory Animals (Rockville, National Institute of Health/Office for Protection from Research Risks, 1996). The study protocol was approved by the Subcommittee for Laboratory Animal Welfare of National Cardiovascular Center.

Human data were retrospectively sampled from an existing database at National Cardiovascular Center which documented subjects who underwent PET examination after the ^{15}O-steady-state protocol. There were 231 total samples, with body weight and age ranging from 58 ± 10 kg, and 63 ± 14 years, respectively. Only the arterial $^{15}O_2$ and $H_2^{15}O$ radioactivity concentrations measured at the steady-state condition were used for the present analysis.

Experimental Protocol

The six monkeys were anesthetized using propofol (4 mg/kg/h) and vecuronium (0.05 mg/kg/h) assigned as a baseline in contrast to the after physiologically stimulated conditions. Animals were intubated and their respiration was controlled by an anesthetic ventilator (Cato, Drager, Germany). Each monkey inhaled 2,200 MBq $^{15}O_2$ for 20 secs. After 3 mins, the monkeys were injected with 370 MBq $H_2^{15}O$ for 30 secs by the anterior tibial vein. This was aimed at assessing both CBF and $CMRO_2$ according to the DARG technique (Kudomi *et al*, 2005). At 30 secs before inhaling $^{15}O_2$ to the monkeys, arterial blood was withdrawn from the femoral artery for 420 secs at a rate of 0.45 mL/min using a Harvard pump (Harvard Apparatus, Holliston, MA, USA). The whole blood TAC was measured with a continuous monitoring system (Kudomi *et al*, 2003) and the $A_i(t)$ was obtained. Meanwhile, we also manually obtained 0.5 mL of arterial blood samples from the contralateral femoral artery at 30, 50, 70, 90, 110, 130, 160, 190, and 360 secs after the $^{15}O_2$ inhalation. For the analysis of sampled blood, 0.2 mL of the blood were used for measurement of the radioactivity concentration of the whole blood, and the rest of the blood sampled (~0.3 mL) was immediately centrifuged for separation to measure the plasma radioactivity concentration ($A_{plasma}(t)$, Bq/mL). The radioactivity concentration was measured using a well counter (Molecular Imaging Laboratory Co. Ltd, Suita, Japan).

In two monkeys, anesthetic level was changed by altering the injection dose of propofol from 4 (baseline) to 8 and then to 12 and 16 mg/kg/h in one monkey, and to 5 and then to 7, 10, and 15 mg/kg/h in the other. In another monkey, $PaCO_2$ level was varied from 39 (baseline) to 47, and then to 33, 26, and 42 mm Hg by changing the respiratory rate. Each measurement for $^{15}O_2$ inhalation and $H_2^{15}O$ injection was initiated after at least 30 mins of applying the physiologic stimulation to achieve a steady state. All procedures were the same as those for the baseline, with the exception of the manual blood sample, which was obtained only once at 70 secs.

Before and after 6 mins of the $^{15}O_2$ inhalation, oxygen concentration in both inhaled (Fi_{O_2}, %) and end-tidal expiratory gas (Fe_{O_2}, %) was measured by the anesthetic ventilator in five out of the six monkeys. Using the respiration rate (r, per min) and the stroke volume (v, mL) indicated on the ventilator, the $BMRO_2$ (R_{O_2} mL/min) was calculated using the following equation:

$$R_{O_2} = (Fi_{O_2} - Fe_{O_2}) \cdot v \cdot r.$$

All monkeys received a PET measurement to assess the $CMRO_2$ at physiologically baseline condition. The scan protocol followed the DARG technique (Kudomi *et al*, 2005) in which a 6-mins single dynamic PET scan was performed in conjunction with the administration of dual tracers (i.e., $^{15}O_2$ followed by $H_2^{15}O$ after a 3-mins interval). PET scanner used was ECAT HR (Siemens-CTI, Knoxville, TN, USA), which provided 47 tomographic slice images for an axial field-of-view of approximately 150 mm. We performed arterial–sinus blood sampling to obtain a global OEF (OEF_{A-V}) (A–V difference approach). We sampled 0.2 mL of arterial and sinus blood simultaneously during each PET scan and measured their oxygen content (C_aO_2 and C_vO_2, respectively) (Kudomi *et al*, 2005). The OEF_{A-V} was calculated as: $OEF_{A-V} = (C_aO_2 - C_vO_2)/C_aO_2$.

With regards to the farm pigs involved in this experiment, we used existing data, which were originally obtained in one of the myocardial projects. During the study, three farm pigs were anesthetized. Anesthesia was induced by ketamine (10 mg/kg) and maintained using propofol (4 mg/kg/h). Animals were intubated and their respiration was controlled by the anesthetic ventilator. Venous blood was labeled with $^{15}O_2$ using a small artificial lung unit (Magata *et al*, 2003). $^{15}O_2$-labeled blood (222 to 700 MBq) was injected for 10 secs via anterior tibial vein. At 30 secs before this injection, arterial blood was withdrawn from the femoral artery at a rate of 0.45 mL/min using the Harvard pump and continued for 420 secs. The whole blood TAC ($A_i(t)$) was then measured with a continuous monitoring system (Kudomi *et al*, 2003). Meanwhile, we manually sampled 0.5 mL of arterial blood from the contralateral femoral artery at 30, 60, 90, 90, 120, 180, 240, and 300 secs after the $^{15}O_2$-labeled blood injection. For the analysis of sampled blood, 0.2 mL of the blood were used for measurement of the radioactivity concentration of the whole blood, and the rest of the blood sampled (~0.3 mL) was immediately centrifuged for separation to measure the plasma radioactivity ($A_{plasma}(t)$, Bq/mL). The radioactivity was measured using the well counter.

Data for rats were also originally obtained for other projects, and only the blood counts were used in this study. Anesthesia was induced with pentobarbital (50 mg/kg). A 10 mL of venous blood was labeled $^{15}O_2$ using a small artificial lung unit as described previously (Magata *et al*, 2003), and approximately 1 mL of $^{15}O_2$-labeled blood (37 to 74 MBq) was injected for 30 secs via the tail vein. Arterial blood samples of 0.1 mL each were obtained from the femoral artery at 5-secs intervals for 60 secs and 10-secs intervals for another 60 secs after the injection. Whole blood radioactivity concentration was measured using the well counter to be used as $A_i(t)$. Arterial blood samples of

0.2 mL each were obtained at 30, 60, 90, and 120 secs, and the plasma radioactivity concentration ($A_{plasma}(t)$) was measured by the well counter.

For clinical patients, the blood radioactivity concentration was obtained from previously performed PET examinations, which followed the steady-state protocol (Hirano *et al*, 1994). Each patient inhaled both $^{15}O_2$ and $C^{15}O_2$ to reach the steady state with an inhalation dose of approximately 1,200 and 500 MBq/min, respectively. Five to seven arterial blood samples were obtained during the steady state from the brachial artery. Mean values of radioactivity concentration of the whole blood and plasma, $A_t(t)$ and $A_{plasma}(t)$, respectively, were obtained for both $^{15}O_2$ and $C^{15}O_2$ PET examination.

Data Analysis

Using the blood activity data obtained from monkeys, pigs, and rats at baseline conditions, k as well as Δt, k_w and p were first determined by the 4PF approach, in which Equation 2 was applied to fit the $A_w(t)$ using the observed $A_t(t)$. Because the solubility of the oxygen is negligibly small in the plasma, we assumed that all radioactivity in plasma fraction comes from $H_2^{15}O$ and that the water content ratio of whole blood to plasma (R) does not change during measurement, which means that the kinetics of water molecules immediately reach equilibrium between the plasma and the cellular fraction (Mintun *et al*, 1984; Iida *et al*, 1993). Thus, $A_w(t)$ was obtained from the equation: $A_w(t) = A_{plasma}(t) \cdot R$, where R value was obtained from the sampled blood at the end of the scan (at which all the radioactivity in the blood can be considered as coming from $H_2^{15}O$ because inhaled $^{15}O_2$ is all metabolized).

Given that the values of Δt, k_w, and p were averages determined from 4PF for monkeys, pigs, and rats, only k was determined by fitting Equation 2 to A_w. This was calculated at various points in time, more specifically, in 30, 50, 70, 90, 110, 130, 160, and 190 secs for monkeys, in 30, 60, 90, 90, 120, 180, and 240 secs for pigs, and in 30, 60, 90, and 120 secs for rats. The optimal time point for k under the 1PF approach was determined, so that $(k_{4PF}-k_{1PF})/k_{4PF}$ reaches a minimal value. Here, k_{4PF} and k_{1PF} denote k values determined by the 4PF and 1PF approaches, respectively. The values of k in monkeys at baseline condition, together with those in pigs and rats were compared between 4PF and 1PF approaches, in which a k value from the optimal single time point was used.

In three of the monkeys, which were physiologically stimulated, k of 1PF approach was obtained using single time point of A_w. Assuming the total blood volume (V_{TB}) for monkeys as 360 mL (Lindstedt and Schaeffer, 2002), and using Hb as measured value in each experiment, k_{BM} was calculated from R_{O_2} according to Equation 7b. Then, k_{BM} obtained as: $k_{BM} = 0.00204 R_{O_2}$ was compared with k determined by 1PF.

For clinical data obtained from the steady-state (SS approach) PET examinations, Equation 6 was used to determine the k values of the SS approach for each patient, in which values of k_1 and k_2 were 0.38 and 0.29 per min as obtained in a previous work by Huang *et al* (1991).

$CMRO_2$ and OEF values in monkeys at baseline condition were calculated using the RW TACs obtained by four different methods (i.e., directly measured $A_w(t)$ ($n=6$), 4PF ($n=6$), 1PF ($n=6$), and BM approaches ($n=5$)). Regions-of-interest were selected for over the whole brain, and $CMRO_2$ and OEF values were obtained in those regions-of-interest. The $CMRO_2$ values compared among the four methods mentioned above to estimate RW TACs. The Bland–Altman method was applied to analyze the agreement of OEF values between the methods. Also, OEF values were compared with OEF_{A-V}.

All data were presented as mean ± 1 standard deviation. Student's t-test was used and Pearson's regression analysis was applied to compare two variables. A probability value of <0.05 was considered statistically significant.

Results

Figure 1 shows results from the simulation study, and shows the magnitude of errors in $CMRO_2$ calculated by the DARG method as well as errors in the parameters, k, Δt, k_w, and p. Errors in $CMRO_2$ were most sensitive to errors in k amongst all species, namely the production rate constant of RW in the arterial blood. After errors in k, errors in $CMRO_2$ were sensitive to errors in Δt. Errors in k_w and p, however, appeared to cause relatively insignificant errors in $CMRO_2$. More specifically, only 5 to 10% errors are caused in $CMRO_2$ by a change of ± 50% in k_w and p.

Figures 2A–2C show examples of the arterial whole blood curves (A_t) and RW TAC (A_w) observed in typical studies on a monkey, a pig, and a rat, respectively. The RW curves became constant after a period in all species. The rise time or appearance of the RW curves, $A_w(t)$, was significantly delayed compare to that of whole blood curve, $A_t(t)$. $A_w(t)$ curves fitted by 4PF well reproduced the measured RW curves in three species: monkeys, pigs, and rats. Table 2 summarizes values of k, Δt, k_w, and p obtained by the four parameter fitting (4PF approach), at the baseline for monkeys, pigs, and rats, and also k value obtained by the steady-state formula for clinical patients. Those comparisons showed that the k was significantly different among species ($P<0.001$) except between pig and human subjects, and it was significantly lower in smaller animals. Likewise, Δt showed significant differences among the three species ($P<0.001$), and it was also lower in smaller animals.

Table 3 summarizes k and $CMRO_2$ values obtained from a series of PET experiments performed on six monkeys at baseline condition, and for increased anesthesia (in two monkeys), and changed $PaCO_2$ levels (in one monkey). The best agreement of k values between 4PF and 1PF approaches was obtained from the blood sample data taken at 60, 70, and 60 secs in pigs, monkeys, and rats, respectively, and was used in the 1PF approach. With this

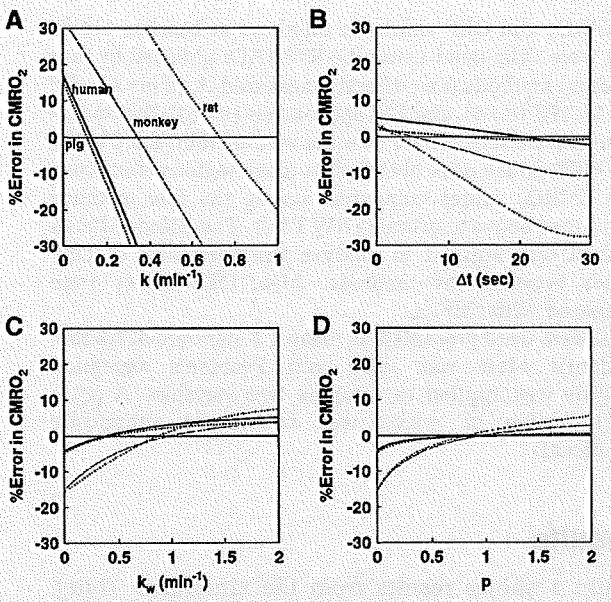

Figure 1 Error in $CMRO_2$ values due to errors in **(A)** k, **(B)** Δt, **(C)** k_w, and **(D)** p for assumed human, pig, monkey and rat. The same type of line indicates the same species. The percentage differences in the $CMRO_2$ values from the assumed true values (Table 1) were plotted as a function of the simulated value of k, Δt, k_w, and p.

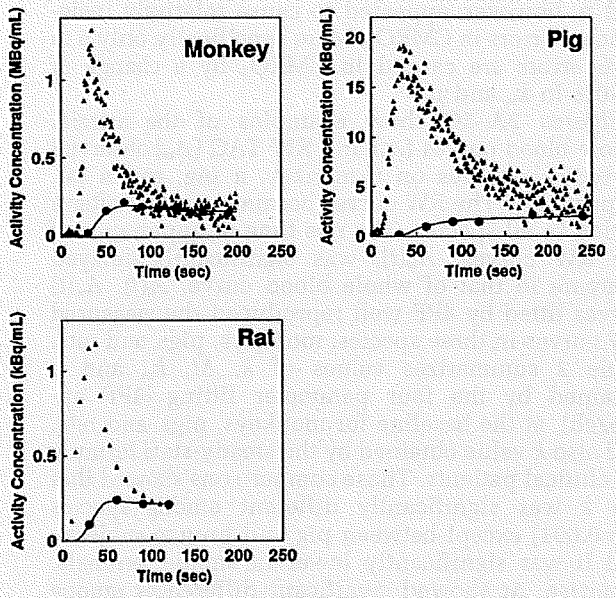

Figure 2 Representative comparison of the measured arterial whole blood and RW time activity curves for monkey, pig, and rat. Closed triangles and closed circles represent the measured whole blood and RW time activity curves, respectively. Estimated time activity curves by 4PF approach were also plotted in a solid line, and indicated a good agreement with the measured one.

optimized calibration protocol, k values were in a good agreement between 4PF and 1PF approaches. As shown in Figure 3, the regression analysis showed significant correlation for 21 animals including 6 monkeys, 3 pigs, and 12 rats ($P<0.001$), and there was no significant difference between the two variables. Figure 4 shows that k values calculated by the 1PF approach (at an optimized time) were in a good agreement with those calculated with the $BMRO_2$. Namely, the regression analysis showed significant correlation ($P<0.001$, $n=16$) and also that there was no significant difference between the two variables. Note that, in the $CMRO_2$ calculation by $BMRO_2$, k values were normalized according to the regression line shown in Figure 4. It should also be noted that calculated $CMRO_2$ values at the baseline shown in Table 3 were not significantly different among the four techniques. The average ($\pm$s.d.) values of obtained OEF were 0.53 ± 0.08, 0.52 ± 0.09, 0.54 ± 0.08, 0.54 ± 0.09, and 0.56 ± 0.04 from A–V difference, directly RW measured approach, 4PF, 1PF, and BM approaches, respectively. The Bland–Altman analysis of OEF values between from A–V difference and from others showed small over/underestimation, that is., with bias $\pm$ s.d. of -0.02 ± 0.09, 0.01 ± 0.07, 0.01 ± 0.08, and 0.02 ± 0.09, by direct RW, 4PF, 1PF, and BM approaches, respectively. Neither of the current methods (direct RW, 4PF, 1PF, and BM) was significantly different from A–V difference approach.

Discussion

Our study showed that the mathematical formula based on the physiologic model that reproduced the time-dependent concentration of RW in the arterial blood after a short-period inhalation of $^{15}O_2$ is indeed adequate. Our approach also simplified the procedures for sequential assessment of RW in $^{15}O_2$ inhalation PET studies, although previous approaches required frequent blood samples and centrifuges of each arterial blood sample. The present approach is an extension of a previous study by Iida *et al* (1993) and Huang *et al* (1991). It is essential if one intends to apply the rapid $^{15}O_2$ PET technique (Kudomi *et al*, 2005) to pharmacologic and physiologic stress studies on a wide range of species. Because the PET acquisition period can be prolonged > 3 mins, statistical accuracy can be significantly improved as compared with Ohta *et al* (1992) and other researchers (Fujita *et al*, 1999; Vafaee and Gjedde, 2000; Okazawa *et al*, 2001*a*, *b*; Yamauchi *et al*, 2003; Mintun *et al*, 2002), under which to avoid effects of RW, the data acquisition period was limited only to < 3 mins (Meyer *et al*, 1987; Ohta *et al*, 1992).

The present RW formula consists of three rate parameters of the production rate of RW in the arterial blood (k), and the forward and backward diffusion rate constants of RW between the blood and the peripheral tissues. The k was presumed to correspond to the oxygen metabolism in the total body system, $BMRO_2$, and was in fact shown to be

Table 2 Averaged values of k, Δt, k_w, and p for monkeys, pigs, rat, and human subjects under baseline condition

	Weight (kg)	k *(per min)*	*Δt (secs)*	k_w *(per min)*	p
Monkey	5.2 ± 0.8^a	0.34 ± 0.16^a	4.5 ± 1.4^a	0.98 ± 0.48	0.98 ± 0.30
Pig	38 ± 9^a	$0.11 \pm 0.02^{a,b}$	10.8 ± 1.8^a	0.83 ± 0.19	1.01 ± 0.26
Rat	0.30 ± 0.054^a	0.73 ± 0.16^a	2.9 ± 1.7^a	0.87 ± 0.30	0.83 ± 0.32
Human	58 ± 10^a	$0.129 \pm 0.023^{a,b}$	—	—	—

Monkey: $n = 6$; pig: $n = 3$; rat: $n = 12$; and human: $n = 231$. Measured values were obtained by 4PF for monkey, pig, rats, whereas those for human were obtained using data in a steady-state method.

[a]Denotes $P < 0.001$ for other species.

[b]Denotes that the difference was not significant in k between pig and human subjects.

Table 3 Values of k and $CMRO_2$ in the whole brain region for monkeys under physiologically baseline and stimulated conditions

ID	*Condition*	k *(per min)*			*$CMRO_2$ (mL/min per 100 g)*			
		4PF	*1PF*	*$BMRO_2$*	*Reference*	*4PF*	*1PF*	*$BMRO_2$*
1	BL	0.36	0.42	—	3.7	3.7	3.6	—
2	BL	0.62	0.66	1.24	3.0	3.3	3.4	3.4
3	BL	0.32	0.39	0.83	3.0	3.1	3.0	2.9
	(Dose of propofol)							
4	BL	0.21	0.18	0.55	2.0	2.0	2.0	1.8
	8 mg/kg/h	—	0.30	0.69	—	—	—	—
	12 mg/kg/h	—	0.23	0.52	—	—	—	—
	16 mg/kg/h	—	0.16	0.40	—	—	—	—
5	BL	0.12	0.15	0.31	2.1	2.1	2.0	1.8
	5 mg/kg/h	—	0.15	0.32	—	—	—	—
	7 mg/kg/h	—	0.16	0.35	—	—	—	—
	10 mg/kg/h	—	0.18	0.36	—	—	—	—
	15 mg/kg/h	—	0.071	0.29	—	—	—	—
	($PaCO_2$ level)							
6	BL	0.43	0.46	0.95	2.8	3.1	3.0	3.3
	47 mm Hg	—	0.20	0.64	—	—	—	—
	33 mm Hg	—	0.21	0.46	—	—	—	—
	26 mm Hg	—	0.14	0.28	—	—	—	—
	42 mm Hg	—	0.33	0.82	—	—	—	—

4PF, four parameters fitting; 1PF, one parameter fitting; $BMRO_2$, total body metabolic rate of oxygen; BL, baseline condition.
Reference: RW TAC was obtained using measured RW data at a baseline condition in all monkeys ($n = 6$). No statistically significant differences were found in $CMRO_2$ between reference and other techniques.

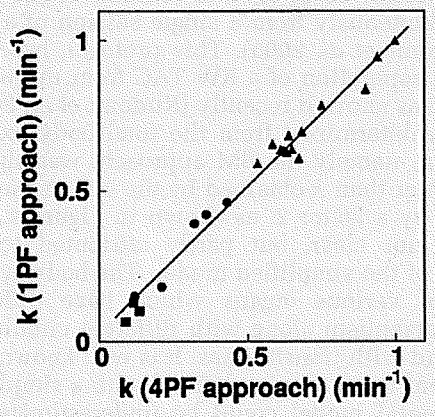

Figure 3 Comparison of the production rates of RW (k, per min) obtained by 4PF and those by 1PF. Squares, circles, and triangles correspond to pigs, monkeys, and rats, respectively. The regression line was $y = 0.97x + 0.026$ (per min) ($r = 0.98$).

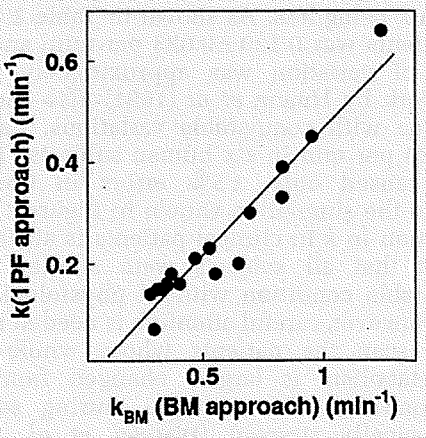

Figure 4 Comparison of the production rates of RW obtained by BM approach and those by 1PF approach in five monkeys at various anesthetic and $PaCO_2$ levels. The regression line was $y = 0.50x - 0.034$ (per min) ($r = 0.95$).

significantly correlated to $BMRO_2$, as measured from the trachea gas sampling (Figure 4). The latter two parameters (k_w and p) appeared to be consistent and did not differ across various species (Table 2). Also, change in those parameters was less sensitive in $CMRO_2$ (Figure 1). These findings suggest that the production of RW after inhalation of $^{15}O_2$ could be described only by a single parameter of k, as shown in Figure 3, although further studies are required to validate this because the method was only tested in a group with small number of subjects of particular physiologic situation (under anesthesia) and has not been applied to different populations. It is also important to note that this parameter (k) estimated from the $BMRO_2$ (i.e., BM approach) provided $CMRO_2$, which was consistent with the trachea gas samplings shown in Figure 4, and that the obtained OEF values by the approaches of 4PF, 1PF, and BM applied in the present study were not significantly different to that by A–V difference approach as revealed by Bland–Altman analysis.

The simulation study also showed that the most sensitive parameter in $CMRO_2$ was the RW production rate constant, k, followed by Δt. It was therefore suggested that k could be determined with a single blood sampling procedure using the 1PF approach, in which other parameter values were determined and fixed from results from the 4PF approach. It was further showed that k could be obtained from the BM approach as determined from oxygen concentration in the expiration gas. Both 1PF and BM approaches appeared to be robustly useful in $^{15}O_2$ PET for assessing quantitative $CMRO_2$ and CBF in clinical studies.

It is important to note that k varies significantly depending on the physiologic status even in the same species, as seen in Figure 4. According to the simulation study in Figure 1, this variation causes nonnegligible errors in $CMRO_2$, if a constant k is used. Changes in k from 0.1 to 0.6 per min causes errors in $CMRO_2$ of $\pm 30\%$ in anesthetized monkeys. Results from clinical studies, however, showed the variation in k being less. As shown in Table 2, k for clinical patients was 0.129 ± 0.023 per min, and the coefficient of variation was approximately 18%. Previous work by Huang *et al* (1991) also showed similar value with comparable variations, namely 0.131 ± 0.026 per min in six human subjects. These variations caused only $\pm 5\%$ errors in $CMRO_2$, according to the simulation shown in Figure 1. The small variation in k in clinical patients is attributed to the fact that all subjects were studied at a relatively stable condition without physiologic stimulation. However, careful attention is needed if one intends to scan the patients whose whole-body oxygen metabolism is largely changed from the baseline condition. For example, during several pharmacologically stressed (Wessen *et al*, 1997; Kaisti *et al*, 2003), exercise-induced physically stressed, and hyper- or hypothermia (Sakoh and Gjedde, 2003) conditions.

The simulation also showed that size of errors in $CMRO_2$ increased in smaller animals, where the value of k was larger. Recently, $CMRO_2$ as well as CBF have been measured in rats using a small animal PET scanner (Magata *et al*, 2003; Yee *et al*, 2006). Magata *et al* performed multiple blood samplings and plasma separation for multiple blood samples to estimate the RW in their experiment involving rats. The procedures were crucial, but have caused serious alterations of physiologic condition in heart pressure and heart rate due to large amount of blood samples for small animals. Our proposed simplified technique for estimating RW from a single blood sample or from $BMRO_2$, is essential for small animals to be able to maintain the physiologic status. The calculation of $CMRO_2$ also requires whole blood arterial TAC, which can be obtained from arterial blood samplings and could change the physiologic condition. However, such blood sampling could also be avoided by an arterial–venous bypass (Weber *et al*, 2002; Laforest *et al*, 2005), by placing a probe in femoral artery (Pain *et al*, 2004), or by a noninvasive method (Yee *et al*, 2006).

Mintun *et al* (1984) has proposed a simple procedure for RW correction based on a linear interpolation for the bolus $^{15}O_2$ inhalation 60-secs PET scan. As shown in Figure 2, the RW curve is not linear particularly in smaller animals, and a systematic error may be caused or scan duration is limited. Ohta *et al* (1992) and other investigators (Ohta *et al*, 1992; Fujita *et al*, 1999; Vafaee and Gjedde, 2000; Okazawa *et al*, 2001*a*, *b*; Yamauchi *et al*, 2003; Mintun *et al*, 2002), however, have used a technique which does not take into account the RW contribution. Only initial short-period data, namely the 3 mins after the bolus inhalation of $^{15}O_2$, were used in their approach, and thus estimated parameters suffered from statistical uncertainties. The present methodology to estimate RW in the arterial blood allows the prolongation of a PET acquisition period. The technique can also be applicable to the recently proposed sequential administration protocol of $^{15}O_2$ followed by $H_2^{15}O$ to estimate $CMRO_2$ and CBF simultaneously from a single session of a PET scan (Kudomi *et al*, 2005). This protocol, however, required a separation of a RW TAC from the whole blood TAC as showed recently (Kudomi *et al*, 2007).

The k_{BM} determined from the total body oxygen metabolism, namely the BM approach, was significantly greater than k obtained by the 4PF or the 1PF approach, by a factor 2, as shown in Figure 4. The reason is not clear, but partly attributed to the limitation of the simplified model. The body system consists of various organs which have different oxygen metabolism along with different circulation systems and with transit times. It is well known that the apparent rate constant defined with a simplified compartmental model could be underestimated as compared with an average of true rate constants, known as heterogeneity effects (Iida *et al*, 1989; Aston *et al*, 2002). This is, however, not essential.

Simply, linear correction could be applied to convert to the apparent k value as has been performed in this study. $CMRO_2$ values calculated using BM approach for the RW separation, were in good agreement with those determined with the direct measurement of RW as shown in Table 3.

The current method with modeling approach and simplified procedure provided consistent results in terms of time-dependent RW component, and consequently metabolic product of $^{15}O_2$ was separated from arterial whole blood for the $CMRO_2$ assessment in PET examination. The modeling approach to separate metabolite from authentic tracer has been showed previously for 6-[^{18}F]fluoro-L-dopa study (fdopa) (Huang *et al*, 1991). We expect that the modeling approach in conjunction with the simplified method showed in our study could be applied for various kinds of tracers, which require the separation of metabolic product such as fdopa. This approach enables us to assess parametric images for those tracers by eliminating the laborious procedures and by avoiding the amount of blood samplings, particularly for smaller animals.

In conclusion, the present RW model was feasible to reproduce RW TAC from a whole radioactivity concentration curve obtained after $^{15}O_2$ inhalation, and for a wide range of species. The simplified procedure to predict the RW TAC is of use to calculate $CMRO_2$ in smaller animals as well as clinical patients.

Acknowledgements

We acknowledge Mr N Ejima for operating the cyclotron and daily maintenance of CTI ECAT HR. We also gratefully thank Ms Atra Ardekani for her invaluable help on preparing the present paper. We also thank the staff of the Investigative Radiology, Research Institute, National Cardiovascular Center, especially, Dr T Inomata, Dr H Jino, Dr N Kawachi, and Dr T Zeniya for their assistance.

References

Aston JA, Cunningham VJ, Asselin MC, Hammers A, Evans AC, Gunn RN (2002) Positron emission tomography partial volume correction: estimation and algorithms. *J Cereb Blood Flow Metab* 22:1019–34

Eriksson L, Holte S, Bohm Chr, Kesselberg M, Hovander B (1988) Automated blood sampling system for positron emission tomography. *IEEE Trans Nucl Sci* 35:703–7

Eriksson L, Kanno I (1991) Blood sampling devices and measurements. *Med Prog Technol* 17:249–57

Fujita H, Kuwabara H, Reutens DC, Gjedde A (1999) Oxygen consumption of cerebral cortex fails to increase during continued vibrotactile stimulation. *J Cereb Blood Flow Metab* 19:266–71

Hayashi T, Watabe H, Kudomi N, Kim KM, Enmi J, Hayashida K, Iida H (2003) A theoretical model of oxygen delivery and metabolism for physiologic interpretation of quantitative cerebral blood flow and metabolic rate of oxygen. *J Cereb Blood Flow Metab* 23:1314–23

Hirano T, Minematsu K, Hasegawa Y, Tanaka Y, Hayashida K, Yamaguchi T (1994) Acetazolamide reactivity on ^{123}I-IMP single photon emission computed tomography in patients with major cerebral artery occlusive disease: correlation with positron emission tomography parameters. *J Cereb Blood Flow Metab* 14:763–70

Holden JE, Eriksson L, Roland PE, Stone-Elander S, Widen L, Kesselberg M (1988) Direct comparison of single-scan autoradiographic with multiple-scan least-squares fitting approaches to PET $CMRO_2$ estimation. *J Cereb Blood Flow Metab* 8:671–80

Huang SC, Barrio JR, Yu DC, Chen B, Grafton S, Melega WP, Hoffman JM, Satyamurthy N, Mazziotta JC, Phelps ME (1991) Modelling approach for separating blood time-activity curves in positron emission tomographic studies. *Phys Med Biol* 36:749–61

Iida H, Jones T, Miura S (1993) Modeling approach to eliminate the need to separate arterial plasma in oxygen-15 inhalation positron emission tomography. *J Nucl Med* 34:1333–40

Iida H, Kanno I, Miura S, Murakami M, Takahashi K, Uemura K (1989) A determination of the regional brain/blood partition coefficient of water using dynamic positron emission tomography. *J Cereb Blood Flow Metab* 9:874–85

Kaisti KK, Langsjo JW, Aalto S, Oikonen V, Sipila H, Teras M, Hinkka S, Metsahonkala L, Scheinin H (2003) Effects of sevoflurane, propofol, and adjunct nitrous oxide on regional cerebral blood flow, oxygen consumption, and blood volume in humans. *Anesthesiology* 99:603–13

Kudomi N, Choi C, Watabe H, Kim KM, Shidahara M, Ogawa M, Teramoto N, Sakamoto E, Iida H (2003) Development of a GSO detector assembly for a continuous blood sampling system. *IEEE Trans Nucl Sci* 50:70–3

Kudomi N, Hayashi T, Teramoto N, Watabe H, Kawachi N, Ohta Y, Kim KM, Iida H (2005) Rapid quantitative measurement of $CMRO_2$ and CBF by dual administration of ^{15}O-labeled oxygen and water during a single PET scan—a validation study and error analysis in anesthetized monkeys. *J Cereb Blood Flow Metab* 25:1209–24

Kudomi N, Watabe H, Hayashi T, Iida H (2007) Separation of input function for rapid measurement of quantitative $CMRO_2$ and CBF in a single PET scan with a dual tracer administration method. *Phys Med Biol* 52: 1893–908

Laforest R, Sharp TL, Engelbach JA, Fettig NM, Herrero P, Kim J, Lewis JS, Rowland DJ, Tai YC, Welch MJ (2005) Measurement of input functions in rodents: challenges and solutions. *Nucl Med Biol* 32:679–85

Lindstedt L, Schaeffer PJ (2002) Use of allometry in predicting anatomical and physiological parameters of mammals. *Lab Anim* 36:1–19

Magata Y, Temma T, Iida H, Ogawa M, Mukai T, Iida Y, Morimoto T, Konishi J, Saji H (2003) Development of injectable O-15 oxygen and estimation of rat OEF. *J Cereb Blood Flow Metab* 23:671–6

Meyer E, Tyler JL, Thompson CJ, Redies C, Diksic M, Hakim AM (1987) Estimation of cerebral oxygen utilization rate by single-bolus 15O2 inhalation and dynamic positron emission tomography. *J Cereb Blood Flow Metab* 7:403–14

Mintun MA, Raichle ME, Martin WR, Herscovitch P (1984) Brain oxygen utilization measured with O-15 radio-

tracers and positron emission tomography. *J Nucl Med* 25:177–87

Mintun MA, Vlassenko AG, Shulman GL, Snyder AZ (2002) Time-related increase of oxygen utilization in continuously activated human visual cortex. *Neuroimage* 16:531–7

Ohta S, Meyer E, Thompson CJ, Gjedde A (1992) Oxygen consumption of the living human brain measured after a single inhalation of positron emitting oxygen. *J Cereb Blood Flow Metab* 12:179–92

Okazawa H, Yamauchi H, Sugimoto K, Takahashi M, Toyoda H, Kishibe Y, Shio H (2001*a*) Quantitative comparison of the bolus and steady-state methods for measurement of cerebral perfusion and oxygen metabolism: positron emission tomography study using 15O-gas and water. *J Cereb Blood Flow Metab* 21:793–803

Okazawa H, Yamauchi H, Sugimoto K, Toyoda H, Kishibe Y, Takahashi M (2001*b*) Effects of acetazolamide on cerebral blood flow, blood volume, and oxygen metabolism: a positron emission tomography study with healthy volunteers. *J Cereb Blood Flow Metab* 21:1472–9

Pain F, Laniece P, Mastrippolito R, Gervais P, Hantraye P, Besret L (2004) Arterial input function measurement without blood sampling using a beta-microprobe in rats. *J Nucl Med* 45:1577–82

Sakoh M, Gjedde A (2003) Neuroprotection in hypothermia linked to redistribution of oxygen in brain. *Am J Physiol Heart Circ Physiol* 285:H17–25

Shidahara M, Watabe H, Kim KM, Oka H, Sago M, Hayashi T, Miyake Y, Ishida Y, Hayashida K, Nakamura T, Iida H (2002) Evaluation of a commercial PET tomograph-based system for the quantitative assessment of rCBF, rOEF and rCMRO2 by using sequential administration of 15O-labeled compounds. *Ann Nucl Med* 16:317–27

Temma T, Magata Y, Kuge Y, Shimonaka S, Sano K, Katada Y, Kawashima H, Mukai T, Watabe H, Iida H, Saji H (2006) Estimation of oxygen metabolism in a rat model of permanent ischemia using positron emission tomography with injectable^{15}O-O_2. *J Cereb Blood Flow Metab* 26:1577–83

Vafaee MS, Gjedde A (2000) Model of blood-brain transfer of oxygen explains nonlinear flow-metabolism coupling during stimulation of visual cortex. *J Cereb Blood Flow Metab* 20:747–54

Votaw JR, Shulman SD (1998) Performance evaluation of the Pico-Count flow-through detector for use in cerebral blood flow PET studies. *J Nucl Med* 39:509–15

Weber B, Burger C, Biro P, Buck A (2002) A femoral arteriovenous shunt facilitates arterial whole blood sampling in animals. *Eur J Nucl Med Mol Imaging* 29: 319–23

Wessen A, Widman M, Andersson J, Hartvig P, Valind S, Hetta J, Langstrom B (1997) A positron emission tomography study of cerebral blood flow and oxygen metabolism in healthy male volunteers anaesthetized with eltanolone. *Acta Anaesthesiol Scand* 41:1204–12

Yamauchi H, Okazawa H, Kishibe Y, Sugimoto K, Takahashi M (2003) The effect of acetazolamide on the changes of cerebral blood flow and oxygen metabolism during visual stimulation. *Neuroimage* 20:543–9

Yee SH, Lee K, Jerabek PA, Fox PT (2006) Quantitative measurement of oxygen metabolic rate in the rat brain using microPET imaging of briefly inhaled 15O-labelled oxygen gas. *Nucl Med Commun* 27:573–81

利用技術

小動物の高解像度SPECTイメージング

銭谷　勉　Zeniya Tsutomu
飯田　秀博　Iida Hidehiro
（国立循環器病センター研究所 先進医工学センター 放射線医学部）

1　はじめに

創薬や新規治療法の評価を目的とした前臨床研究において，マウスやラットを用いた小動物の *in vivo* イメージングは，同一の動物を非侵襲的に繰り返し検査できる点から，その要求は高い。特に，PET（Positron Emission Tomography）やSPECT（Single Photon Emission Computed Tomography）といった核医学検査装置は，高い感度でトレーサの挙動を観測できるため，病態生理や病態生化学的な変化を定量的に評価できる。遺伝子改変したマウスなどのイメージングにおいて，その利用価値が高いと考えられる。

実際に小動物を撮像する場合，サイズがヒトよりも相当小さいため，高い空間解像度が要求される。SPECT装置の場合，ピンホールコリメータの拡大効果を利用することで比較的容易に高い解像度が得られる。現在，実用化されているほとんどの小動物用SPECT装置はピンホールコリメータを採用している。

本稿では，小動物の高解像度SPECTイメージング技術及び我々の開発した小動物用SPECT装置を紹介し，最後にピンホールSPECTのヒトへの応用について述べる。

2　ピンホールコリメータを利用した高解像度SPECT

SPECT装置は原理的に放射性同位元素から放出されるγ線の飛来方向を特定するためのコリメータを必要とする。臨床用のSPECT装置では，一般的にパラレルホールコリメータが用いられており，解像度は10 mm程度である。小動物イメージングでは対象臓器も小さいため，それに伴って，高解像度が要求される。図1のようにピンホールコリメータは撮像対象がコリメータに近いほど，小視野領域の像をより拡大できるため，空間解像度及び感度を高くで

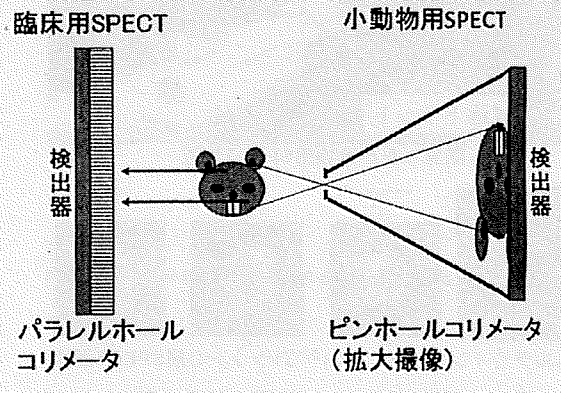

図1　ピンホールコリメータによる拡大撮像

きる。1 mm 以下の解像度も比較的容易に実現できるため，小動物のイメージングに適している。

ピンホールコリメータを利用する技術は古くからあったが，研究の域を脱しなかった。それは，ピンホール SPECT で得られる画像は体軸方向に歪み，視野内で解像度が不均一になるため，定量評価が困難であったからである。我々はこの原因をデータの不完全に由来するものと仮説をたて，完全データを収集する撮像軌道を構築し，この軌道に対応する統計学に基づいた3次元画像再構成法を開発した。これによって，歪みのない視野全体で均一な解像度を有する3次元画像を得ることが可能になった（図2）[1]。画像歪を改善する手法としては，他に，ヘリカル軌道による完全データ収集法，多数のピンホールを配列した近似的な完全データを収集する手法が開発されている。ただし，従来の撮像軌道でも統計学的3次元画像再構成を利用すれば視野の中央付近であれば歪みはある程度改善される。

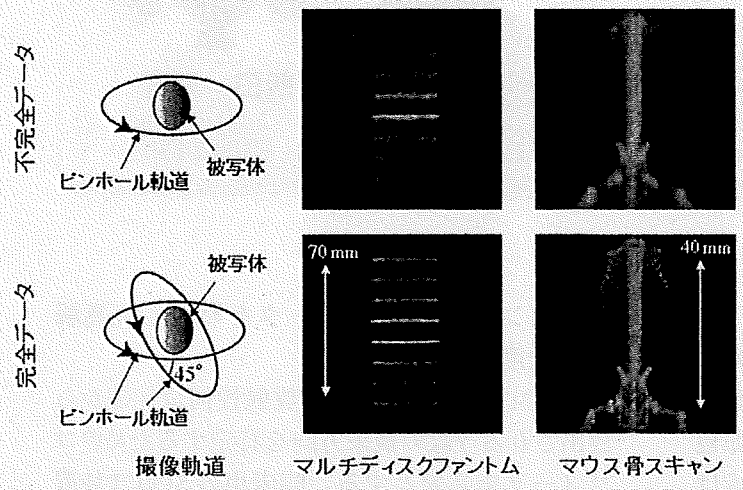

図2　従来の単一円軌道による不完全データ（上）と2軸収集軌道による完全データ（下）から得られた再構成画像

3　小動物用 SPECT 装置

我々は，小型で可搬性のある小動物専用 SPECT 装置を開発した。装置を小型化するために導入した小型高解像度検出器は，大きさ 5 cm 程度であり，シンチレータが臨床用の平板 NaI に代えて，1.5 mm ピッチのピクセル型 NaI で，光電子増倍管（Photomultiplier Tube：PMT）も従来の2あるいは3インチの大型 PMT に代えて，6 mm の PMT で構成されている。小型高解像度検出器とピンホールコリメータの拡大撮像技術を組み合わせて[2]，コンパクトな小動物専用高解像度 SPECT 装置を開発した（図3(a)）。本装置では，ピンホールコリメータの弱点でもある低感度を補うため，被写体の周囲に4台の検出器が 90° 間隔で配列されている。また，小動物ベッドが水平方向に回転可能となっており，異なる回転軸による撮像軌道で完全データ収集が可能である。

マルチラインソースファントム実験では，1.3 mm 径のラインが識別可能であった（図3(b)）。また，本装置を用いて，覚醒下で，健常ラットの心筋血流量及び血管反応性が評価可能であることを実証した。図3(c)は本実験で

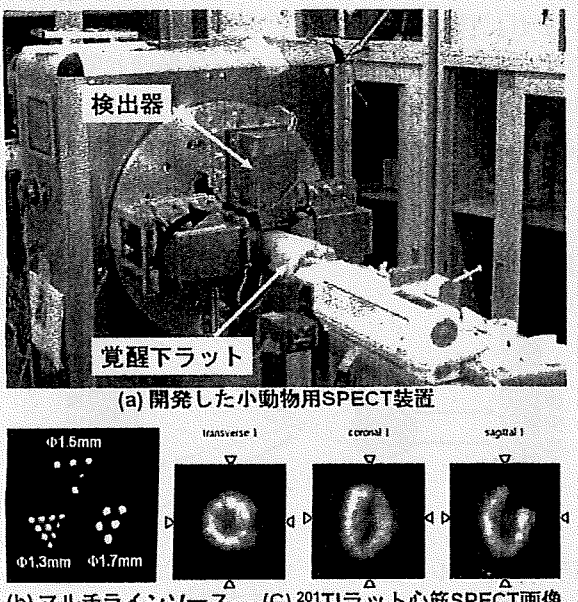

図3　小動物用 SPECT 装置と再構成画像

得られたラット心筋SPECT画像であるが，非常に鮮明である。

4 ピンホールSPECTによるヒト局所高解像度撮像

従来，ピンホールSPECTのような小視野でヒトのような大きな被写体を撮像した場合，データ欠損(トランケーション)が生じ，それによるアーチファクトや過大評価のため，定量評価は困難であった。そこで，我々はピンホールSPECTにおいてトランケーションを許す画像再構成法を開発した[3]。図4のように視野内に被写体の外側のゼロカウント領域（既知領域）を含むこと，画像再構成領域が被写体全体を含むこと，この2つの条件下で逐次近似による画像再構成を行うことによって，視野内はトランケーションの影響なく，正しい画像が得られる。このことを脳ファントム実験によって実証した（図4）。臨床SPECTでは低解像度で詳細構造は見えなかった。また，ピンホールSPECTデータを従来法で再構成した場合はアーチファクトが見られ，視野全域でカウントが過大評価されていた。一方，ピンホールSPECTデータを開発した手法で画像再構成した場合，アーチファクトも過大評価もなく，高解像度で詳細構造が描出された。

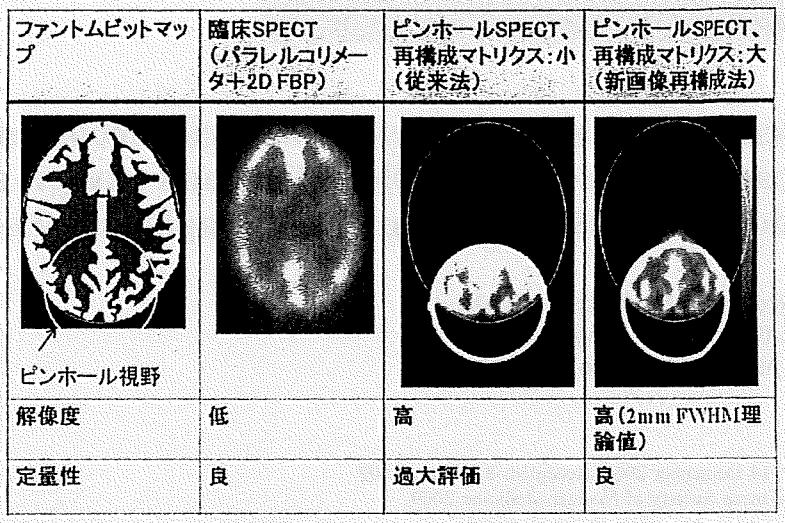

図4 脳ファントムの再構成画像
ピンホールSPECTと新再構成法によって，アーチファクトや過大評価がなく，詳細構造が明瞭に描出された

本撮像技術によって，微小腫瘍検出，血管プラークイメージング，てんかん焦点同定，部分容積効果のない血流定量などが可能になると考えられる。

5 おわりに

現在，小動物の高解像度SPECTイメージングはピンホールコリメータと撮像法の工夫によって実用化の域に達した。さらに，小動物撮像で培われた高解像度技術はヒトの撮像へ応用されようとしている。

参考文献

1) Zeniya T, *et al.*: *Eur J Nucl Med Mol Imaging*, **31**, 1166-1172 (2004)
2) Zeniya T, *et al.*: *Ann Nucl Med*, **20**, 409-416 (2006)
3) Zeniya T, *et al.*: *IEEE 2007 Nuclear Science Symposium Conference Record*, **6**, 4205-4207 (2007)

Ann Nucl Med
DOI 10.1007/s12149-009-0243-7

ORIGINAL ARTICLE

Influence of residual oxygen-15-labeled carbon monoxide radioactivity on cerebral blood flow and oxygen extraction fraction in a dual-tracer autoradiographic method

Katsuhiro Iwanishi · Hiroshi Watabe · Takuya Hayashi · Yoshinori Miyake · Kotaro Minato · Hidehiro Iida

Received: 14 December 2008 / Accepted: 8 January 2009

Abstract
Objective Cerebral blood flow (CBF), cerebral metabolic rate of oxygen ($CMRO_2$), oxygen extraction fraction (OEF), and cerebral blood volume (CBV) are quantitatively measured with PET with ^{15}O gases. Kudomi et al. developed a dual tracer autoradiographic (DARG) protocol that enables the duration of a PET study to be shortened by sequentially administrating $^{15}O_2$ and $C^{15}O_2$ gases. In this protocol, before the sequential PET scan with $^{15}O_2$ and $C^{15}O_2$ gases ($^{15}O_2$–$C^{15}O_2$ PET scan), a PET scan with $C^{15}O$ should be preceded to obtain CBV image. $C^{15}O$ has a high affinity for red blood cells and a very slow washout rate, and residual radioactivity from $C^{15}O$ might exist during a $^{15}O_2$–$C^{15}O_2$ PET scan. As the current DARG method assumes no residual $C^{15}O$ radioactivity before scanning, we performed computer simulations to evaluate the influence of the residual $C^{15}O$ radioactivity on the accuracy of measured CBF and OEF values with DARG method and also proposed a subtraction technique to minimize the error due to the residual $C^{15}O$ radioactivity.

Methods In the simulation, normal and ischemic conditions were considered. The $^{15}O_2$ and $C^{15}O_2$ PET count curves with the residual $C^{15}O$ PET counts were generated by the arterial input function with the residual $C^{15}O$ radioactivity. The amounts of residual $C^{15}O$ radioactivity were varied by changing the interval between the $C^{15}O$ PET scan and $^{15}O_2$–$C^{15}O_2$ PET scan, and the absolute inhaled radioactivity of the $C^{15}O$ gas. Using the simulated input functions and the PET counts, the CBF and OEF were computed by the DARG method. Furthermore, we evaluated a subtraction method that subtracts the influence of the $C^{15}O$ gas in the input function and PET counts.

Results Our simulations revealed that the CBF and OEF values were underestimated by the residual $C^{15}O$ radioactivity. The magnitude of this underestimation depended on the amount of $C^{15}O$ radioactivity and the physiological conditions. This underestimation was corrected by the subtraction method.

Conclusions This study showed the influence of $C^{15}O$ radioactivity in DARG protocol, and the magnitude of the influence was affected by several factors, such as the radioactivity of $C^{15}O$, and the physiological condition.

Keywords PET · OEF · CBV · Carbon monoxide

K. Iwanishi (✉) · H. Watabe · T. Hayashi · H. Iida
Department of Investigative Radiology, National Cardiovascular Center Research Institute, 5-7-1 Fujishirodai, Suita, Osaka 565-8565, Japan
e-mail: kiwanish@ri.ncvc.go.jp

Y. Miyake
Department of Radiology and Nuclear Medicine, National Cardiovascular Center, Osaka, Japan

K. Iwanishi · K. Minato
Infomatics Science, Nara Institute of Science and Technology, Nara, Japan

Published online: 10 April 2009

Introduction

Positron emission tomography with ^{15}O gas can quantitatively measure cerebral blood flow (CBF), oxygen extraction fraction (OEF), cerebral metabolic rate of oxygen ($CMRO_2$), and cerebral blood volume (CBV). These functional values are important clinical indices that can be used to evaluate ischemic degree mainly in chronic cerebral arterial occlusive diseases. Several quantitative approaches

have been developed to obtain CBF and $CMRO_2$ images based on a single-tissue compartment model for oxygen and water kinetics [1–4]. In the steady-state method [5–9], quantitative images are estimated from data acquired while in the steady state reached during the continuous inhalation of $^{15}O_2$ and $C^{15}O_2$. The study period with this method is long (approximately 2 h) due to the waiting time needed to reach equilibrium. The autoradiographic method, which uses separate administrations of three traces of CO, CO_2, and O_2 (three-step ARG), has also been employed [3, 10–14]. The study period with the ARG method is shorter than that need with the steady-state method. However, a study with the ARG method still takes more than half an hour, because there is a waiting time for the decay of the residual radioactivity of the preceding tracer used.

Previously, Kudomi et al. developed a dual tracer autoradiographic (DARG) method to shorten the PET study period [15, 16]. This method used a single PET scan with sequential administration of dual tracers of $^{15}O_2$ and $C^{15}O_2$ ($^{15}O_2$–$C^{15}O_2$ scan), and computed CBF and $CMRO_2$ simultaneously in an autoradiographic manner. Although the DARG approach eliminated the waiting time of radioactivity decay between $^{15}O_2$ and $C^{15}O_2$ administrations, a separate PET scan with $C^{15}O$ is required for obtaining a CBV image and correction of blood volume in $CMRO_2$ before the DARG scan. However, between these scans for $C^{15}O$ and the DARG we need another waiting time for the radioactivity decay of $C^{15}O$, since the DARG approach itself does not take into account the residual $C^{15}O$ radioactivity in the arterial input function (AIF) and PET data. Furthermore, CO has a relatively long biological clearance from the blood due to high affinity to hemoglobin. While it is desired to further decrease the waiting time for the decay in the actual clinical study, it has not been defined how long it should be, and how small amount of the residual activity will affect the accuracy of CBF and $CMRO_2$.

In this study, we performed computer simulations and evaluated the influence of this residual $C^{15}O$ radioactivity on the CBF and OEF values obtained by the DARG method. Moreover, we proposed a method to remove the influence of the $C^{15}O$ on the DARG method calculation (Subtraction method).

Materials and methods

Computation of functional values

CBF and OEF values were calculated from tissue TAC [$C_i(t)$] and AIF during an $^{15}O_2$–$C^{15}O_2$ scan, based on a single-tissue compartment model for oxygen and water, and the DARG method [15]. Using the method developed by Kudomi et al. [16], the AIF was separated into $^{15}O_2$ ($A_{O_2}(t)$) and $H_2^{15}O$ ($A_{H_2O}(t)$) (Note that although we used $C^{15}O_2$ gas, we used $H_2^{15}O$ for the expression in this section due to the rapid exchange of $H_2^{15}O$ by carbonate dehydratase in the lung). The total radioactivity in the tissue after the $^{15}O_2$ and $C^{15}O_2$ administration can be expressed as,

$$Ci(t) = f \cdot A_{H_2O}(t) \otimes \exp^{-\frac{f}{p}t} + E \cdot f \cdot A_{O_2}(t) \otimes \exp^{-\frac{f}{p}t} + V_B \cdot R_{Hct}(1 - Fv \cdot E) A_{O_2}(t) \quad (1)$$

where f is CBF, E is the OEF, p is the blood/tissue partition coefficient of water, R_{Hct} is the small-to-large vessel hematocrit ratio, and V_B is the cerebral blood volume. F_v is the effective venous fraction. The first term of the right-hand side describes the amount of water entering the tissue. The second term represents the amount of oxygen that enters the tissue and is immediately metabolized to water. The third term is the radioactivity of the $^{15}O_2$ in the blood vessels.

V_B is separately calculated using data from a $C^{15}O$ scan and the following equation [13]:

$$V_B = \frac{C_{CO}}{R_{Hct} \cdot \rho_{brain} \cdot RI_{CO} \cdot \rho_{blood}}. \quad (2)$$

ρ_{brain} and ρ_{blood} represent the densities of blood (=1.06 g/mL) and brain tissue (=1.04 g/mL). RI_{CO} (Bq/mL) is the mean of the radioactivity concentration for $C^{15}O$ in the arterial blood.

To calculate functional values using a look-up table procedure, Eq. 1 was integrated for the periods after the $H_2^{15}O$ (represents $\int_W$) and $^{15}O_2$ administration (represents $\int_O$) as

$$\begin{aligned} \int_W Ci(t)dt &= f \int_W A_{H_2O}(t) \otimes \exp^{-\frac{f}{p}t} dt \\ &\quad + E \cdot f \int_W A_{O_2}(t) \otimes \exp^{-\frac{f}{p}t} dt + V_B \\ &\quad \cdot R_{Hct}(1 - Fv \cdot E) \int_W A_{O_2}(t)dt \\ \int_O Ci(t)dt &= f \int_O A_{H_2O}(t) \otimes \exp^{-\frac{f}{p}t} dt \\ &\quad + E \cdot f \int_O A_{O_2}(t) \otimes \exp^{-\frac{f}{p}t} dt + V_B \\ &\quad \cdot R_{Hct}(1 - Fv \cdot E) \int_O A_{O_2}(t)dt \end{aligned} \quad (3)$$

From the above equation, E can be expressed as follows:

$$E = \frac{\int_o Ci(t) - f \int_o A_{H_2O} \otimes \exp^{-\frac{f}{p}t} dt - V_B \cdot R_{Hct} \int_o A_{O_2} dt}{f \int_o A_{O_2} \otimes \exp^{-\frac{f}{p}t} dt - V_B \cdot R_{Hct} \cdot Fv \int_o A_{O_2} dt}. \quad (4)$$

Substituting Eq. 4 into Eq. 3, we obtain

$$\int_w \mathrm{Ci}(t)\mathrm{d}t = f\int_w A_{\mathrm{H_2O}}(t)\otimes\exp^{-\frac{f}{P}t}\mathrm{d}t + V_\mathrm{B}\cdot R_\mathrm{Hct}\int_w A_{\mathrm{O_2}}(t)\mathrm{d}t + \left(f\int_w A_{\mathrm{O_2}}(t)\otimes\exp^{-\frac{f}{P}t}\mathrm{d}t - V_\mathrm{B}\cdot R_\mathrm{Hct}\cdot\mathrm{Fv}\int_w A_{\mathrm{O_2}}(t)\mathrm{d}t\right) \times \frac{\int_o \mathrm{Ci}(t) - f\int_o A_{\mathrm{H_2O}}\otimes\exp^{-\frac{f}{P}t}\mathrm{d}t - V_\mathrm{B}\cdot R_\mathrm{Hct}\int_o A_{\mathrm{O_2}}\mathrm{d}t}{f\int_o A_{\mathrm{O_2}}\otimes\exp^{-\frac{f}{P}t}\mathrm{d}t - V_\mathrm{B}\cdot R_\mathrm{Hct}\cdot\mathrm{Fv}\int_o A_{\mathrm{O_2}}\mathrm{d}t}. \quad (5)$$

Using Eq. 5, f can be estimated using a look-up table procedure based on the integration value of the tissue TAC and separated input function. Next, E can be calculated using Eq. 4.

Study protocol with DARG method

Figure 1 shows a schematic diagram of the clinical study protocol with the DARG method for our institute. The PET scanner we used was an ECAT EXACT47 (CTI Inc., Knoxville, USA). First, a 10 min transmission scan was performed to correct for gamma ray attenuation. Then gaseous $C^{15}O$ of 2500 MBq was inhaled for 30 s, and 90 s post-inhalation, a 4 min emission scan ($C^{15}O$ scan) was performed to obtain a CBV image. Finally, a single dynamic PET scan was conducted during the sequential administration of gaseous $^{15}O_2$ (4000 MBq) and $C^{15}O_2$ (5000 MBq) in a short time interval. Their inhalation times were 1 min.

A catheter was inserted into the brachial artery of the patient. The arterial blood was sampled at the beginning of the $C^{15}O$ scan for 30 s and the radioactivity concentration in the arterial blood was measured by a Well counter system (Shimadzu Corporation, Kyoto, JAPAN). In order to obtain the AIF, the radioactivity in the arterial blood during a $^{15}O_2$–$C^{15}O_2$ scan was continuously monitored by a GSO detector [17] with a flow rate of 3.5 mL/min. The inner diameter of the tube was approximately 2 mm, and the distance from the catheter to the detector was 20–25 cm.

Residual $C^{15}O$ radioactivity

As described in the "Introduction", the AIF and PET counts obtained during a DARG study may be contaminated by residual $C^{15}O$ radioactivity. By assuming that the $C^{15}O$ was physically decayed but not biologically cleared, the radioactivity of the $C^{15}O$ in the AIF and PET counts during the O_2–CO_2 scan could be quantified. The residual radioactivity of the $C^{15}O$ [$R_{CO}(0)$ (Bq/mL)] in the AIF at the start time of the O_2–CO_2 can be written as follows:

$$R_\mathrm{CO} = A_\mathrm{CO}\cdot\exp(-\lambda T), \quad (6)$$

where A_{CO} (Bq/mL) is the measured arterial radioactivity for $C^{15}O$ by the Well counter and λ is the physical decay constant for ^{15}O (0.005670 s^{-1}).

PET counts from the residual $C^{15}O$ (C_{CO}) were calculated from R_{CO} and the measured CBV (V_B) by $C^{15}O$ scan from Eq. 2 as follows

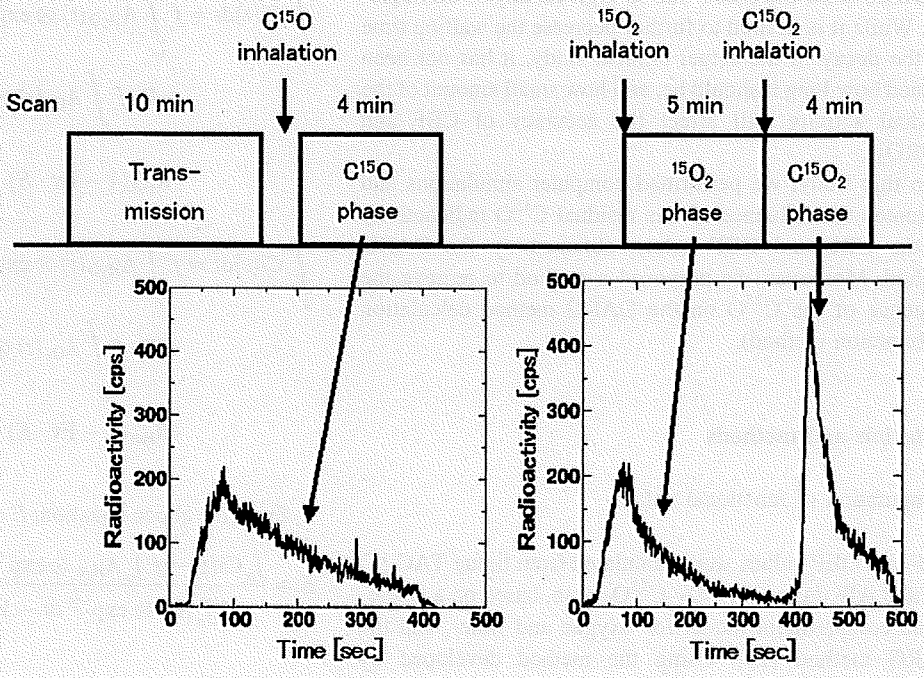

Fig. 1 Schematic diagram of PET study with DARG method protocol. After a 10 min transmission scan, $C^{15}O$ gas is inhaled for 30 s before the start of a 4 min scan. There is approximately 10 min in the administration interval for $C^{15}O$ and $^{15}O_2$. Next, a 9 min single scan with sequential administration of $^{15}O_2$ and $C^{15}O_2$ is performed. The administration interval between $^{15}O_2$ and $C^{15}O_2$ is 300 s. The graphs below are arterial input functions without corrections for decay, delay, and scaling for $C^{15}O$ (*left*), $^{15}O_2$ and $C^{15}O_2$ (*right*)

$$C_{CO} = R_{CO} \cdot \rho_{blood} \cdot \rho_{brain} \cdot R_{Hct} \cdot V_B. \quad (7)$$

We proposed a subtraction method that eliminates the influence of the $C^{15}O$ radioactivity in both the AIF and PET counts during the O_2–CO_2 scan. The true AIF (A_{True}) of the $^{15}O_2$–$C^{15}O_2$ at time t was obtained by subtracting R_{CO} from the measured whole radioactivity [$A_{whole}(t)$], i.e.,

$$A_{True}(t) = A_{Whole}(t) - R_{CO}. \quad (8)$$

Note that $A_{True}(t)$ and $A_{Whole}(t)$ were corrected for the physical decay of ^{15}O against the scan start time 0. PET counts without the residual CO radioactivity could be obtained by subtracting C_{co} in Eq. (7) from the observed PET counts as follows:

$$C_{True}(t) = C_i(t) - C_{co}. \quad (9)$$

Using $A_{True}(t)$ and $C_{True}(t)$, CBF and OEF were calculated in the DARG manner.

Simulation studies

As shown in Eq. 1, DARG calculation does not take into count the residual radioactivity of the CO. However, in an actual situation, both the PET count [Ci(t)] and the input function (A_{O_2} and A_{H_2O}) might contain radioactivity from the $C^{15}O$. So, the CBF and OEF values calculated by the DARG method are influenced by the $C^{15}O$ radioactivity, causing error and noise in the terms of Eq. 1. Computer simulations were performed to evaluate this influence. Both normal and ischemic models were considered in these simulations. Moreover, the effect of the subtraction method was examined.

The simulations were performed using a PC [CPU: Intel (R) Pentium (R) 4 2.80 GHz, OS: Linux Fedora Core 7] with a PyBLD environment [18].

Simulated input function with CO radioactivity

We used a typical arterial input function from one patient's data for the simulations. From the measured input function, the input functions with $C^{15}O$ radioactivity (combined input function, CIF) were generated using Eq. 6. The amount of residual $C^{15}O$ radioactivity was varied by changing two conditions, the time lag between the $C^{15}O$ scan and the $^{15}O_2$–$C^{15}O_2$ scan (T in Eq. 6), and the $C^{15}O$ radioactivity against the $^{15}O_2$ radioactivity (A_{co} in Eq. 6). The time lags selected were 60, 100, 200, 400, and 800 s, and the inhaled $C^{15}O$ radioactivity was either 25% (case '25%') or 100% (case '100%') of the $^{15}O_2$ inhaled radioactivity. 100 sets of noisy arterial TACs for $C^{15}O$ were realized by assuming that the standard deviation of the $C^{15}O$ radioactivity was equal to the square root of the $C^{15}O$ radioactivity. Figure 2 (left) shows the CIF after $^{15}O_2$ gas inhalation in a case where the time lag was 60 s. These TACs did not correct the physiological decay of $^{15}O_2$. For the subtraction method, $A_{True}(t)$ in Eq. 8 was computed for each dataset.

Simulated tissue TAC with CO radioactivity

Using the typical input function and Eq. 1, the tissue TAC during a $^{15}O_2$–$C^{15}O_2$ scan was simulated. We considered two physiological conditions, namely the normal condition

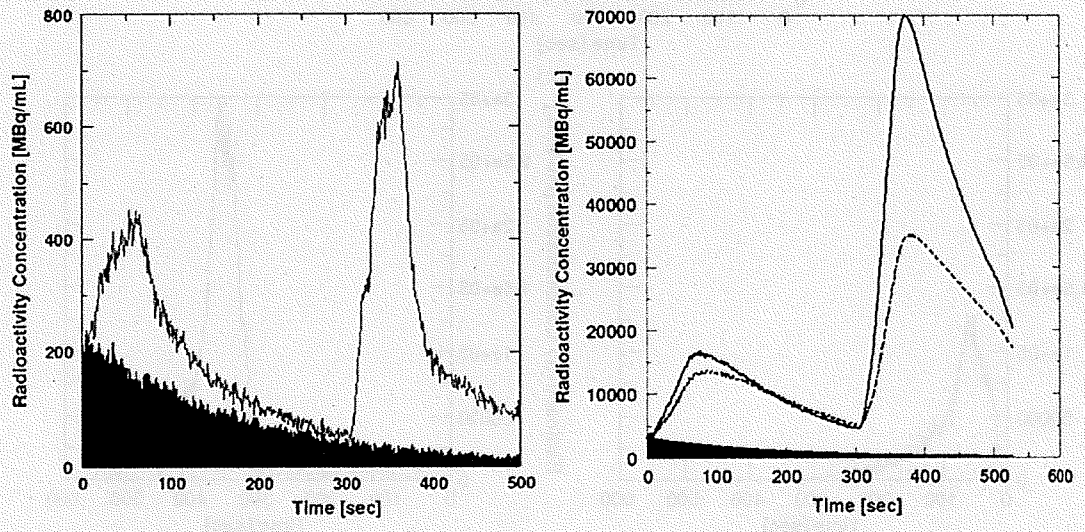

Fig. 2 Input function (*left*) and PET count curves (*right*) during the $^{15}O_2$–$C^{15}O_2$ scan. These curves have the added residual $C^{15}O$ radioactivity (hatched region). The interval time for the $C^{15}O$ and $^{15}O_2$ is 60 s, and the inhaled $C^{15}O$ radioactivity is 100% of the peak value for $^{15}O_2$. $C^{15}O$ time-activity curve. The *solid line* in the *right graph* indicates the PET counts in the normal model, and the *dashed line* is the PET counts in the ischemic model